HHS Public Access

Author manuscript

Science. Author manuscript; available in PMC 2016 September 04.

Published in final edited form as:

Science. 2016 March 4; 351(6277): 1043–1048. doi:10.1126/science.aad2450.

CryoEM structure of a native, fully glycosylated and cleaved HIV-1 envelope trimer

Jeong Hyun Lee[1,2,3], **Gabriel Ozorowski**[1,2,3], and **Andrew B. Ward**[1,2,3,*]

[1]Department of Integrative Structural and Computational Biology, The Scripps Research Institute, La Jolla, CA 92037, USA.

[2]Center for HIV/AIDS Vaccine Immunology and Immunogen Discovery, The Scripps Research Institute, La Jolla, CA 92037, USA.

[3]International AIDS Vaccine Initiative Neutralizing Antibody Center and Collaboration for AIDS Vaccine Discovery, The Scripps Research Institute, La Jolla, CA 29037, USA.

Abstract

The envelope glycoprotein trimer (Env) on the surface of HIV-1 recognizes CD4+ T cells and mediates viral entry. During this process, Env undergoes large conformational rearrangements making it difficult to study in its native state. Soluble, stabilized trimers have provided valuable insights into Env structure, but they lack the hydrophobic membrane proximal external region (MPER), which is an important target of broadly neutralizing antibodies (bnAbs), the transmembrane domain and the cytoplasmic tail (CT). Here we present a 4.2 Å resolution cryoEM structure of a clade B virus Env lacking only the cytoplasmic tail (EnvΔCT) and stabilized by the bnAb PGT151, and an 8.8 Å resolution reconstruction of EnvΔCT in complex with PGT151 and MPER-targeting antibody 10E8. These structures provide new insights into the wild-type Env structure.

One Sentence Summary

The high-resolution cryoEM structures of a membrane-derived HIV-1 envelope glycoprotein trimer reveal the native structure, glycosylation, and the epitopes of broadly neutralizing antibodies PGT151 and 10E8, and provides an important comparator for soluble SOSIP trimers being developed as vaccine candidates.

The HIV-1 envelope glycoprotein (Env) houses the receptor binding site and fusion machinery to infect target cells. The intrinsic instability and glycosylation on Env have made high-resolution structure determination a daunting task. Low-resolution tomographic reconstructions of Env on the viral surface have described the overall shape of the trimer (1, 2) and more recently structures of an engineered, soluble clade A BG505 SOSIP.664 trimer

*Correspondence to: abward@scripps.edu.

Supplementary Materials:

Materials and Methods
Figs. S1 to S16
Table S1
References (44–64)

have been solved at high resolution (3–9). The BG505 SOSIP.664 trimer interacts preferentially with broadly neutralizing antibodies (bnAbs), but not non-neutralizing antibodies (10), and has promising immunogenic properties (11, 12). While these data suggest that this soluble trimer recapitulates native Env it is not known what effect the stabilizing mutations, or lack of MPER and transmembrane domain (TM) have on the Env structure.

SOSIP shares a highly similar architecture with wild-type Env

Here we studied the JR-FL Env strain with the cytoplasmic tail (CT) deleted (subsequently referred to as EnvΔCT). In some isolates the deletion of the CT has been shown to increase exposure of non-neutralizing epitopes (13), but the deletion of CT in JR-FL does not abolish the ability of the trimer to fuse and infect (14, 15). Our previously described protocol (16) for JR-FL EnvΔCT-PGT151 complex extraction was modified to make the sample amenable for cryoEM (fig. S1A–B), resulting in a 4.2 Å resolution reconstruction (Fig. 1A–B, fig. S1–S3). Similar to our negative-stain reconstructions (16), PGT151 Fab bound in an asymmetric manner, with a maximum of 2 Fabs per trimer. Because the three gp140 interfaces were non-equivalent, from hereon, we refer to them as interfaces 1, 2, or 3 (Fig. 1A).

The clade B JR-FL EnvΔCT shares a similar topology to BG505 SOSIP.664, despite the lack of stabilizing mutations and difference in subtypes (68.5% sequence identity) (fig. S4, fig. S5A and E). Differences were observed at the trimer apex, and the N-terminal heptad repeat (HR) 1 region ($HR1_N$) of gp41. In the JR-FL trimer, the inter-V1/V2 loop region of the trimer apex is more loosely associated than in the unliganded BG505 SOSIP.664 (PDB ID: 4ZMJ) (fig. S5B). This phenomenon is consistent with FRET studies of viral Env (17), as well as studies of clades B and C SOSIP.664 trimers where loop mobility and flexibility have been observed (18, 19). Despite this weaker interaction, the V3 loop in all three protomers remains in contact with the base of V2 on the adjacent protomer (fig. S5B and fig. S6A), and therefore likely confers the majority of stability at the trimer apex.

In the published BG505 SOSIP.664 structures $HR1_N$ does not adopt regular secondary structure (4–9), while in our JR-FL EnvΔCT model, this region is helical (fig. S5D). We attribute this difference to the I559P mutation in SOSIP that disrupts the propensity of the HR1 peptide to form an extended and stable α-helix during fusion (20). The “SOS” disulfide bond, on the other hand, does not cause any major conformational differences relative to the wild-type structure (fig. S5C). As in the SOSIP.664 structures (4–9), most of the C-terminus of HR2 is helical until residue 664. Hydrogen deuterium exchange mass spectrometry (HDXMS) studies (21) have however demonstrated that the C-terminal region of HR2 in SOSIP.664 has a flexible topology. While the C-terminal region of gp41 is observed in our JR-FL EnvΔCT structure, the micelle-embedded MPER and TM just downstream of HR2 were both unresolved (Fig. 1A, fig. S1D–E, S2C). Crystal structures of MPER peptide-Fab complexes have also shown that MPER can adopt different conformations (22–24).

Model building of newly resolved regions

We used the BG505 SOSIP.664 and PGT151 Fab x-ray structure coordinates (PDB ID: 4TVP (6) and 4NUG (16), respectively) as starting models for building and refinement (fig. S3, S5F, S6 and table S1). The two previously unmodeled regions in gp41, the fusion peptide (FP, residues 512–527) and $HR1_N$ (548–568) (Fig. 1C, and fig. S4), were both resolved in the current structure. The $HR1_N$ helix in interfaces 2 and 3 was tilted by ~24° away from the center of the trimer, and ~26° to the right in comparison to interface 1 (Fig. 2A), when viewed normal to the threefold axis of the trimer. The $HR1_N$ and $HR1_C$ form a helix-turn-helix type motif, but contain residues with high helical propensity in the turn region (Fig. 2A, and fig. S4). The $HR1_N$ region in the unliganded protomer is less well defined than the liganded $HR1_N$ helices (fig. S5D), as would be expected of a conformationally variable segment.

In the BG505.664 x-ray structure, the N-terminus of the FP (A512–A518) is disordered and appears to project into the solvent. Similarly, at interface 1 of the cryoEM model, residues A512-L520 are unresolved, but density adjacent to $HR1_N$ could be attributed to the FP (fig. S7A), suggesting that the hydrophobic N-terminus of the FP may be inserted into the trimer core in wild-type Env as seen in another class I viral fusion protein, influenza hemagglutinin (HA) (25). At the liganded interfaces, there are changes in both the antibody and the FP. The majority of both the Fab heavy and light chain residues (HC and LC, respectively) adopt the same conformation as when the Fab is unliganded, except for the heavy chain complementarity determining region 3 (CDRH3) of PGT151 (P100a-Y100l), which is substantially different in the two structures (fig. S7B). Upon PGT151 binding, the entire FP is resolved (fig. S7C), where it projects away from the trimer and is sequestered in a pocket formed between the PGT151 Fab CDRH2, CDRH3 and CDRL3 loops via hydrophobic and backbone interactions (Fig. 2B, and fig. S7D). Because the FP is pulled away from the trimer core in both BG505 SOSIP.664 and PGT151-bound Env, which stabilizes the pre-fusion trimer, this conformation of the FP may counter-intuitively contribute to trimer stability.

Newly revealed glycans in the wild-type Env trimer

The Env trimers in our studies contain fully processed, native glycans. Similar to the two other cryoEM structures (5, 9), at least the two core N-acetylglucosamine (GlcNAc) moieties are visible at the majority of glycosylation sites except in disordered peptide regions, such as V1 and V4 (fig. S6B–D, table S1). On the other hand, the glycans in the PGT151 epitope are ordered, allowing us to resolve four highly branched glycans at N241 and N448 in gp120, and N611 and N637 in gp41.

Gp120 glycans have been studied extensively, but much less is known about gp41 glycans. In our structure, glycans at positions N625 and N616 were only resolved up to the core GlcNAc residues (table S1). The ordered glycans at positions N611 and N637 that interact with PGT151 were built as complex glycans with N-acetyllactosamine (LacNAc) branching consistent with published glycan array binding data (Fig. 3A–D, fig. S8 and S9) (26). The base GlcNAc residues of the N611 and N637 glycans were core fucosylated (Fig. 3A–B, fig.

S8 and S9), which agrees with glycan array data demonstrating fucose-dependent binding differences by some clonal relatives of PGT151 (26) and binding studies (fig. S10).

The N611 glycan is minimally a tri-antennary glycan, with the two LacNAc units of the Mannose (Man)(α1–6) arm resolved. The LacNAc(β1–6) branch packs against the heavy chain framework region 3 (FRWH3). The LacNAc(β1–2) interacts with a highly conserved CDRH2 region of the PGT151 family, and also extends far enough to make potential contacts with the FP of the adjacent gp41 (Fig. 3A and C, fig. S8, and fig. S12A–B).

The N637 glycan is a tetra-antennary glycan (Fig. 3B and D, fig. S9) and the core trisaccharide interacts along the length of CDRH3 (Fig. 3B). The interactions are likely backbone mediated, as the PGT151 family CDRH3 sequences in this stretch are variable (fig. S12A and C). The Man(α1–3) branch projects between the HC and LC, with the LacNAc(β1–4) unit primarily interacting with CDRH1, and the LacNAc(β1–2) branch with the C-terminus of CDRL2. The GlcNAc(β1–6)Man(α1–6) branch interacts with another well-conserved region in CDRL2 (Fig. 3B, fig. S12A and C).

Previous low-resolution modeling and glycan knockout neutralization assays allowed us to predict that glycans from N262 and N448 from one gp120 protomer, and N276 from the adjacent gp120 protomer on a BG505 trimer could interact with the PGT151 Fab (16). Here, we see density for a glycan at N241 (glycosylation site ~96% conserved, not present in BG505), which along with the N448 glycan, extend towards FWRH3 (Fig. 3E, fig. S11A and B), The N276 glycan is the least resolved out of the four PGT151 proximal gp120 glycans (fig. S11C), suggesting that it makes considerably fewer contacts relative to N448 or N241, although is positioned to restrict accessibility to the PGT151 epitope.

In TZM-bl neutralization assays, the IC_{50} improved slightly when the N241 or N448 glycan was knocked out in JR-FL pseudovirus (26), corroborating our structural observations. In the same assay, the presence of either N611 or N637 glycan alone in gp41 is sufficient for neutralization, albeit with decreased potency (26). The most intriguing effect was seen with double knockouts. In JR-FL, the reduced neutralization potency due to N637 knockout can be recovered by a second simultaneous knockout of the N448 glycan. This effect is not seen with BG505 pseudovirus, which naturally lacks the N241 glycan. Furthermore, in BG505 pseudovirus, the N637A glycan knockout does not cause as large a decrease in neutralization potency as in JR-FL (26). Together, we hypothesize that the N448 glycan imposes a steric hurdle for PGT151 binding, but only in the presence of the highly conserved N241 glycan (Fig. 4A). The N241 glycan likely limits the range of motion of the N448 glycan, which in turn limits access to the PGT151 epitope, in a similar manner to steric restriction to epitopes by glycans that has been observed with other bnAbs (27–29). It has also been suggested that the presence or lack of one glycan can affect the conformational space that can be occupied by adjacent glycans (30). This type of mechanism illustrates the complex nature of Env surface accessibility and the difficulty of determining complete epitopes outside of high-resolution structures. Lastly, the D2/D3 branch of the very highly conserved N262 oligomannose glycan is in close proximity to the FWRL3 of PGT151, that suggests interactions with the D2 arm, although it is unclear if this glycan is hindering or enhancing PGT151 binding (fig. S11D).

Trimers of different genotypes may contain different glycoforms, especially in gp41 (31) and variation at these sites may be responsible for neutralization plateau (26). Our model illustrates that the PGT151 epitope extends beyond the gp41 glycans and includes gp120 glycans that may also contribute to incomplete neutralization. Overall, PGT151 is highly glycan-dependent, with up to six glycans in JR-FL (N241, N262, N276, N448, N611, N637) surrounding the antibody (Fig. 4A).

Mechanism of trimer stabilization

The most remarkable feature of PGT151 is that, unlike any other identified bnAb so far, including gp41–gp120 interface antibodies, such as 35O22 (32) (fig. S13A), it stabilizes the meta-stable prefusion Env for prolonged periods (16). Contact with both N611 and N637 glycans likely prevent the HR2 helix from progressing to the post-fusion conformation (Fig. 4B). PGT151 and its clonal relatives all have a long CDRL1 of 16 residues, and a conserved N28 (D28 in PGT154–158, fig. S12A) at the CDRL1 tip that interacts with a conserved region at the end of $HR1_N$ (sequence conservation: Q551–Q552: 100%, N553: 58%, N554: 99%). Additionally, CDRH3 is wedged between the $HR1_N$ and the FP proximal HR1 region. In this manner, the CDRL1 and CDRH3 cap the end of a short helix to prevent it from extending into a longer helix and thwarts transition to post-fusion conformation (Fig. 4C). PGT151 has an unusual binding stoichiometry of two Fabs per trimer, even though there is no obvious steric barrier for the third Fab to bind (fig. S13B). Rather, binding of two PGT151 antibodies appears to have an allosteric effect, altering the conformation of the third binding site (Fig. 4D).

10E8 bound conformation of Env

To visualize the MPER, we added 10E8 to the complex and analyzed the JR-FLΔCT-PGT151 Fab-10E8 Fab complex by cryoEM (fig. S14A–B). While 10E8 had some stabilizing effect on the MPER, we still observed flexibility in this region (Fig. 5A, fig. S14C), consistent with a previously solved crystal structure of the MPER peptide-10E8 Fab complex (Fig. 5C) (22). Despite variation in the protein conformation and binding occupancies on the trimer we obtained a 8.8 Å resolution reconstruction from a subset of the JR-FLΔCT-PGT151 Fab-10E8 Fab complexes (Fig. 5A and fig. S14D). This reconstruction revealed that the center of the trimer at the base is empty, similar to the JR-FL EnvΔCT-PGT151 structure. Again, we did not observe a three-helix bundle formed by the TM, but MPER bound to 10E8, and the HR2-MPER interface could now be visualized (Fig. 5B, fig. S15A). The HR2-MPER connectivity was substantially different from the crystal structure (Fig. 5C, and fig. S15A).

10E8 recognizes Env primarily via CDRH3 contacts with MPER helix 672–683, with additional interactions between FWRH3 and the gp41–gp120 interface (Fig. 6A–B). Moreover, N88 and N625 glycans are positioned to sterically block 10E8 binding. The N88 glycan, built as a $ManGlcNAc_2$ in the 4.2 Å model, clashes with FWRH1 and a complete glycan at N625 would also clash with the 10E8 Fab constant region (Fig. 6A–B). Indeed, N625Q mutation increases maximum neutralization of JR2, and glycoforms affect the degree of neutralization plateauing (33). In the trimer structure, both the N88 and N625

glycans are accessible for glycan processing and have been predicted to be complex (34–36). Thus, these glycans could restrict access to the MPER epitope. Most MPER antibodies bind to gp41 fusion intermediates (37–39), but while 10E8 potently neutralizes virus post-CD4 attachment (33), it also neutralizes the pre-fusion trimer (22, 32). Other studies have suggested that the CD4-bound form of Env may be lifted from the membrane, and would therefore provide greater accessibility to membrane proximal epitopes (32). CD4 binding opens Env via a rotation in gp120, which would move the N88 glycan further away from the base of the trimer (Fig. 6C). NMR structures of MPER peptides, as well as our EnvΔCT model (fig. S16A), suggest that the ground state MPER epitope is embedded in the membrane (15). Thus, while difficult to access, MPER antibodies can either bind MPER while membrane embedded or during some transient exposure when the trimer is lifted off the membrane surface. The hydrophilic and likely hydrated base of the trimer (fig. S16B) suggests that the ectodomain is not tightly associated with the membrane.

In the negative stain reconstruction of 10E8 in complex with MPER containing BG505 SOSIP.683 (fig S. 15B–C), the Fab does not induce an opening of the trimer as is seen when soluble CD4, or CD4i antibodies are bound (2). While the 2D class averages of 10E8 bound SOSIP.683 trimers clearly display distinguishable Fab densities (fig. S15B), the particles refine poorly in the 3D reconstruction, and the 10E8 Fab binds at a different angle than in EnvΔCT (fig. S15C), again consistent with MPER flexibility. Without the TM however, the Fab approaches from the bottom of the trimer, which would be impossible in the context of the viral membrane. Cross-linking the ectodomain of full-length Env also has no effect on MPER bnAb binding, despite the reduced CD4 binding (40). Together, these observations overall support that 1) MPER is largely inaccessible on the viral membrane with the membrane imposing a steric hurdle for the Fab approach angle, and 2) 10E8 binds a transiently exposed MPER which is not necessarily the CD4-bound conformation of Env, or a fusion transition conformation, in contrast to previous observations (41). The appearance of a gap between the HR2 C-terminus and the micelle in our 10E8 bound structure (Fig. 5A) likely represents the optimal display of the membrane anchored MPER epitope with all additional constraints in place. The epitope of 10E8, and perhaps of other MPER antibodies is therefore more complex than previously thought, involving elements from multiple gp41 protomers, as well as gp120.

Discussion

Here we present the cryo-EM reconstruction of a cleaved WT JR-FL EnvΔCT trimer in complex with PGT151 Fab at 4.2 Å resolution demonstrating the structure not only of wild-type Env, but also the structure of a type I viral fusion protein with an intact TM, which surprisingly, was found to be flexible. The PGT151 epitope includes the fusion peptide and an extensive network or primary and secondary glycan interactions that stabilize the prefusion conformation of the Env trimer. Intriguingly, the MPER appears sequestered in the detergent micelle in the unliganded state, but is outside the micelle in the 10E8-bound structure, suggesting a dynamic topology. This property, in combination with steric constraints from gp120, gp41, and glycans at N88 and N625 effectively shield the conserved MPER. Thus far, MPER peptide vaccines, while immunogenic, produce non-neutralizing antibodies likely due to the lack of the additional constraints provided by the trimer and

membrane (42, 43), and our model suggests that the minimalistic MPER epitope peptide presentation may not be the most ideal strategy to elicit MPER bnAbs. Overall, our data indicate that Env is a pliable structure where several of the protein-protein interfaces can be remodeled, making it a difficult moving target for the immune system.

Supplementary Material

Refer to Web version on PubMed Central for supplementary material.

Acknowledgments

We thank C. Blattner for the PGT151 and JR-FL EnvΔCT plasmids, J. Torres and N. Overney for helping with plasmid preparations, T. Nieusma for technical assistance, A. Sarkar and L. Kong for advice on glycan modeling, and I. A. Wilson for helpful comments and discussion. The data presented in this manuscript are tabulated in the main paper and in the supplementary materials. The cryoEM reconstructions of JR-FL EnvΔCT-PGT151 and JR-FL EnvΔCT-PGT151-10E8, and the JR-FL EnvΔCT-PGT151 model have been submitted to the PDB and EMDB, with accession codes PDB-5FUU, EMD-3308, EMD-3309 and EMD-3312. This work was supported by the NIH grant UM1 AI100663, the International AIDS Vaccine Initiative Neutralizing Antibody Consortium through the Collaboration for AIDS Vaccine Discovery grants OPP1084519 and OPP1115782, and the California HIV/AIDS Research Program Dissertation Award (to J.H.L.). This work was partially funded by IAVI with the generous support of USAID, Ministry of Foreign Affairs of the Netherlands, and the Bill & Melinda Gates Foundation; a full list of IAVI donors is available at www.iavi.org. The contents of this manuscript are the responsibility of the authors and do not necessarily reflect the views of USAID or the US Government. The EM work was conducted at the Cryo Electron Microscopy Facility at The Scripps Research Institute. This is manuscript number 29175 from the Scripps Research Institute.

References and Notes

1. Liu J, Bartesaghi A, Borgnia MJ, Sapiro G, Subramaniam S. Molecular architecture of native HIV-1 gp120 trimers. Nature. 2008; 455:109–113. published online EpubSep 4. [PubMed: 18668044]
2. Tran EE, Borgnia MJ, Kuybeda O, Schauder DM, Bartesaghi A, Frank GA, Sapiro G, Milne JL, Subramaniam S. Structural mechanism of trimeric HIV-1 envelope glycoprotein activation. PLoS pathogens. 2012; 8:e1002797. [PubMed: 22807678]
3. Julien JP, Lee JH, Cupo A, Murin CD, Derking R, Hoffenberg S, Caulfield MJ, King CR, Marozsan AJ, Klasse PJ, Sanders RW, Moore JP, Wilson IA, Ward AB. Asymmetric recognition of the HIV-1 trimer by broadly neutralizing antibody PG9. Proceedings of the National Academy of Sciences of the United States of America. 2013; 110:4351–4356. published online EpubMar 12. [PubMed: 23426631]
4. Julien JP, Cupo A, Sok D, Stanfield RL, Lyumkis D, Deller MC, Klasse PJ, Burton DR, Sanders RW, Moore JP, Ward AB, Wilson IA. Crystal structure of a soluble cleaved HIV-1 envelope trimer. Science. 2013; 342:1477–1483. published online EpubDec 20. [PubMed: 24179159]
5. Lyumkis D, Julien JP, de Val N, Cupo A, Potter CS, Klasse PJ, Burton DR, Sanders RW, Moore JP, Carragher B, Wilson IA, Ward AB. Cryo-EM structure of a fully glycosylated soluble cleaved HIV-1 envelope trimer. Science. 2013; 342:1484–1490. published online EpubDec 20. [PubMed: 24179160]
6. Pancera M, Zhou T, Druz A, Georgiev IS, Soto C, Gorman J, Huang J, Acharya P, Chuang GY, Ofek G, Stewart-Jones GB, Stuckey J, Bailer RT, Joyce MG, Louder MK, Tumba N, Yang Y, Zhang B, Cohen MS, Haynes BF, Mascola JR, Morris L, Munro JB, Blanchard SC, Mothes W, Connors M, Kwong PD. Structure and immune recognition of trimeric pre-fusion HIV-1 Env. Nature. 2014; 514:455–461. published online EpubOct 23. [PubMed: 25296255]
7. Do Kwon Y, Pancera M, Acharya P, Georgiev IS, Crooks ET, Gorman J, Joyce MG, Guttman M, Ma X, Narpala S, Soto C, Terry DS, Yang Y, Zhou T, Ahlsen G, Bailer RT, Chambers M, Chuang GY, Doria-Rose NA, Druz A, Hallen MA, Harned A, Kirys T, Louder MK, O'Dell S, Ofek G, Osawa K, Prabhakaran M, Sastry M, Stewart-Jones GB, Stuckey J, Thomas PV, Tittley T, Williams C, Zhang B, Zhao H, Zhou Z, Donald BR, Lee LK, Zolla-Pazner S, Baxa U, Schon A, Freire E, Shapiro L, Lee KK, Arthos J, Munro JB, Blanchard SC, Mothes W, Binley JM, McDermott AB, Mascola JR,

Kwong PD. Crystal structure, conformational fixation and entry-related interactions of mature ligand-free HIV-1 Env. Nature structural & molecular biology. 2015; 22:522–531. published online EpubJul.

8. Garces F, Lee JH, de Val N, Torrents de la Pena A, Kong L, Puchades C, Hua Y, Stanfield RL, Burton DR, Moore JP, Sanders RW, Ward AB, Wilson IA. Affinity Maturation of a Potent Family of HIV Antibodies Is Primarily Focused on Accommodating or Avoiding Glycans. Immunity. 2015; 43:1053–1063. published online EpubDec 15. [PubMed: 26682982]
9. Lee JH, de Val N, Lyumkis D, Ward AB. Model Building and Refinement of a Natively Glycosylated HIV-1 Env Protein by High-Resolution Cryoelectron Microscopy. Structure. 2015; 23:1943–1951. published online EpubOct 6. [PubMed: 26388028]
10. Sanders RW, Derking R, Cupo A, Julien JP, Yasmeen A, de Val N, Kim HJ, Blattner C, de la Pena AT, Korzun J, Golabek M, de Los Reyes K, Ketas TJ, van Gils MJ, King CR, Wilson IA, Ward AB, Klasse PJ, Moore JP. A next-generation cleaved, soluble HIV-1 Env trimer, BG505 SOSIP.664 gp140, expresses multiple epitopes for broadly neutralizing but not non-neutralizing antibodies. PLoS pathogens. 2013; 9:e1003618. published online EpubSep. [PubMed: 24068931]
11. Sanders RW, van Gils MJ, Derking R, Sok D, Ketas TJ, Burger JA, Ozorowski G, Cupo A, Simonich C, Goo L, Arendt H, Kim HJ, Lee JH, Pugach P, Williams M, Debnath G, Moldt B, van Breemen MJ, Isik G, Medina-Ramirez M, Back JW, Koff WC, Julien JP, Rakasz EG, Seaman MS, Guttman M, Lee KK, Klasse PJ, LaBranche C, Schief WR, Wilson IA, Overbaugh J, Burton DR, Ward AB, Montefiori DC, Dean H, Moore JP. HIV-1 VACCINES. HIV-1 neutralizing antibodies induced by native-like envelope trimers. Science. 2015; 349:aac4223. published online EpubJul 10. [PubMed: 26089353]
12. Dosenovic P, von Boehmer L, Escolano A, Jardine J, Freund NT, Gitlin AD, McGuire AT, Kulp DW, Oliveira T, Scharf L, Pietzsch J, Gray MD, Cupo A, van Gils MJ, Yao KH, Liu C, Gazumyan A, Seaman MS, Bjorkman PJ, Sanders RW, Moore JP, Stamatatos L, Schief WR, Nussenzweig MC. Immunization for HIV-1 Broadly Neutralizing Antibodies in Human Ig Knockin Mice. Cell. 2015; 161:1505–1515. published online EpubJun 18. [PubMed: 26091035]
13. Chen J, Kovacs JM, Peng H, Rits-Volloch S, Lu J, Park D, Zablowsky E, Seaman MS, Chen B. HIV-1 ENVELOPE. Effect of the cytoplasmic domain on antigenic characteristics of HIV-1 envelope glycoprotein. Science. 2015; 349:191–195. published online EpubJul 10. [PubMed: 26113642]
14. Abrahamyan LG, Mkrtchyan SR, Binley J, Lu M, Melikyan GB, Cohen FS. The cytoplasmic tail slows the folding of human immunodeficiency virus type 1 Env from a late prebundle configuration into the six-helix bundle. Journal of virology. 2005; 79:106–115. published online EpubJan. [PubMed: 15596806]
15. Sun ZY, Cheng Y, Kim M, Song L, Choi J, Kudahl UJ, Brusic V, Chowdhury B, Yu L, Seaman MS, Bellot G, Shih WM, Wagner G, Reinherz EL. Disruption of helix-capping residues 671 and 674 reveals a role in HIV-1 entry for a specialized hinge segment of the membrane proximal external region of gp41. Journal of molecular biology. 2014; 426:1095–1108. published online EpubMar 6. [PubMed: 24075869]
16. Blattner C, Lee JH, Sliepen K, Derking R, Falkowska E, de la Pena AT, Cupo A, Julien JP, van Gils M, Lee PS, Peng W, Paulson JC, Poignard P, Burton DR, Moore JP, Sanders RW, Wilson IA, Ward AB. Structural delineation of a quaternary, cleavage-dependent epitope at the gp41–gp120 interface on intact HIV-1 Env trimers. Immunity. 2014; 40:669–680. published online EpubMay 15. [PubMed: 24768348]
17. Munro JB, Gorman J, Ma X, Zhou Z, Arthos J, Burton DR, Koff WC, Courter JR, Smith AB 3rd, Kwong PD, Blanchard SC, Mothes W. Conformational dynamics of single HIV-1 envelope trimers on the surface of native virions. Science. 2014; 346:759–763. published online EpubNov 7. [PubMed: 25298114]
18. Pugach P, Ozorowski G, Cupo A, Ringe R, Yasmeen A, de Val N, Derking R, Kim HJ, Korzun J, Golabek M, de Los Reyes K, Ketas TJ, Julien JP, Burton DR, Wilson IA, Sanders RW, Klasse PJ, Ward AB, Moore JP. A native-like SOSIP.664 trimer based on an HIV-1 subtype B env gene. Journal of virology. 2015; 89:3380–3395. published online EpubMar. [PubMed: 25589637]
19. Julien JP, Lee JH, Ozorowski G, Hua Y, Torrents de la Pena A, de Taeye SW, Nieusma T, Cupo A, Yasmeen A, Golabek M, Pugach P, Klasse PJ, Moore JP, Sanders RW, Ward AB, Wilson IA.

Design and structure of two HIV-1 clade C SOSIP.664 trimers that increase the arsenal of native-like Env immunogens. Proceedings of the National Academy of Sciences of the United States of America. 2015; 112:11947–11952. published online EpubSep 22. [PubMed: 26372963]

20. Sanders RW, Vesanen M, Schuelke N, Master A, Schiffner L, Kalyanaraman R, Paluch M, Berkhout B, Maddon PJ, Olson WC, Lu M, Moore JP. Stabilization of the soluble, cleaved, trimeric form of the envelope glycoprotein complex of human immunodeficiency virus type 1. Journal of virology. 2002; 76:8875–8889. published online EpubSep. [PubMed: 12163607]
21. Guttman M, Garcia NK, Cupo A, Matsui T, Julien JP, Sanders RW, Wilson IA, Moore JP, Lee KK. CD4-induced activation in a soluble HIV-1 Env trimer. Structure. 2014; 22:974–984. published online EpubJul 8. [PubMed: 24931470]
22. Huang J, Ofek G, Laub L, Louder MK, Doria-Rose NA, Longo NS, Imamichi H, Bailer RT, Chakrabarti B, Sharma SK, Alam SM, Wang T, Yang Y, Zhang B, Migueles SA, Wyatt R, Haynes BF, Kwong PD, Mascola JR, Connors M. Broad and potent neutralization of HIV-1 by a gp41-specific human antibody. Nature. 2012; 491:406–412. published online EpubNov 15. [PubMed: 23151583]
23. Pejchal R, Gach JS, Brunel FM, Cardoso RM, Stanfield RL, Dawson PE, Burton DR, Zwick MB, Wilson IA. A conformational switch in human immunodeficiency virus gp41 revealed by the structures of overlapping epitopes recognized by neutralizing antibodies. Journal of virology. 2009; 83:8451–8462. published online EpubSep. [PubMed: 19515770]
24. Bryson S, Julien JP, Hynes RC, Pai EF. Crystallographic definition of the epitope promiscuity of the broadly neutralizing anti-human immunodeficiency virus type 1 antibody 2F5: vaccine design implications. Journal of virology. 2009; 83:11862–11875. published online EpubNov. [PubMed: 19740978]
25. Wilson IA, Skehel JJ, Wiley DC. Structure of the haemagglutinin membrane glycoprotein of influenza virus at 3 A resolution. Nature. 1981; 289:366–373. published online EpubJan 29. [PubMed: 7464906]
26. Falkowska E, Le KM, Ramos A, Doores KJ, Lee JH, Blattner C, Ramirez A, Derking R, van Gils MJ, Liang CH, McBride R, von Bredow B, Shivatare SS, Wu CY, Chan-Hui PY, Liu Y, Feizi T, Zwick MB, Koff WC, Seaman MS, Swiderek K, Moore JP, Evans D, Paulson JC, Wong CH, Ward AB, Wilson IA, Sanders RW, Poignard P, Burton DR. Broadly neutralizing HIV antibodies define a glycan-dependent epitope on the prefusion conformation of gp41 on cleaved envelope trimers. Immunity. 2014; 40:657–668. published online EpubMay 15. [PubMed: 24768347]
27. Garces F, Sok D, Kong L, McBride R, Kim HJ, Saye-Francisco KF, Julien JP, Hua Y, Cupo A, Moore JP, Paulson JC, Ward AB, Burton DR, Wilson IA. Structural evolution of glycan recognition by a family of potent HIV antibodies. Cell. 2014; 159:69–79. published online EpubSep 25. [PubMed: 25259921]
28. Sok D, Doores KJ, Briney B, Le KM, Saye-Francisco KL, Ramos A, Kulp DW, Julien JP, Menis S, Wickramasinghe L, Seaman MS, Schief WR, Wilson IA, Poignard P, Burton DR. Promiscuous glycan site recognition by antibodies to the high-mannose patch of gp120 broadens neutralization of HIV. Science translational medicine. 2014; 6:236ra263. published online EpubMay 14.
29. Lee JH, Leaman DP, Kim AS, Torrents de la Pena A, Sliepen K, Yasmeen A, Derking R, Ramos A, de Taeye SW, Ozorowski G, Klein F, Burton DR, Nussenzweig MC, Poignard P, Moore JP, Klasse PJ, Sanders RW, Zwick MB, Wilson IA, Ward AB. Antibodies to a conformational epitope on gp41 neutralize HIV-1 by destabilizing the Env spike. Nat Commun. 2015; 6:8167. [PubMed: 26404402]
30. Derking R, Ozorowski G, Sliepen K, Yasmeen A, Cupo A, Torres JL, Julien JP, Lee JH, van Montfort T, de Taeye SW, Connors M, Burton DR, Wilson IA, Klasse PJ, Ward AB, Moore JP, Sanders RW. Comprehensive antigenic map of a cleaved soluble HIV-1 envelope trimer. PLoS pathogens. 2015; 11:e1004767. published online EpubMar. [PubMed: 25807248]
31. Pritchard LK, Spencer DI, Royle L, Vasiljevic S, Krumm SA, Doores KJ, Crispin M. Glycan Microheterogeneity at the PGT135 Antibody Recognition Site on HIV-1 gp120 Reveals a Molecular Mechanism for Neutralization Resistance. Journal of virology. 2015; 89:6952–6959. published online EpubJul. [PubMed: 25878100]
32. Huang J, Kang BH, Pancera M, Lee JH, Tong T, Feng Y, Imamichi H, Georgiev IS, Chuang GY, Druz A, Doria-Rose NA, Laub L, Sliepen K, van Gils MJ, de la Pena AT, Derking R, Klasse PJ,

Migueles SA, Bailer RT, Alam M, Pugach P, Haynes BF, Wyatt RT, Sanders RW, Binley JM, Ward AB, Mascola JR, Kwong PD, Connors M. Broad and potent HIV-1 neutralization by a human antibody that binds the gp41–gp120 interface. Nature. 2014; 515:138–142. published online EpubNov 6. [PubMed: 25186731]

33. Kim AS, Leaman DP, Zwick MB. Antibody to gp41 MPER alters functional properties of HIV-1 Env without complete neutralization. PLoS pathogens. 2014; 10:e1004271. published online EpubJul. [PubMed: 25058619]
34. Cutalo JM, Deterding LJ, Tomer KB. Characterization of glycopeptides from HIV-I(SF2) gp120 by liquid chromatography mass spectrometry. Journal of the American Society for Mass Spectrometry. 2004; 15:1545–1555. published online EpubNov. [PubMed: 15519221]
35. Go EP, Herschhorn A, Gu C, Castillo-Menendez L, Zhang S, Mao Y, Chen H, Ding H, Wakefield JK, Hua D, Liao HX, Kappes JC, Sodroski J, Desaire H. Comparative Analysis of the Glycosylation Profiles of Membrane-Anchored HIV-1 Envelope Glycoprotein Trimers and Soluble gp140. Journal of virology. 2015; 89:8245–8257. published online EpubAug 15. [PubMed: 26018173]
36. Go EP, Hewawasam G, Liao HX, Chen H, Ping LH, Anderson JA, Hua DC, Haynes BF, Desaire H. Characterization of glycosylation profiles of HIV-1 transmitted/founder envelopes by mass spectrometry. Journal of virology. 2011; 85:8270–8284. published online EpubAug. [PubMed: 21653661]
37. Crooks ET, Moore PL, Richman D, Robinson J, Crooks JA, Franti M, Schulke N, Binley JM. Characterizing anti-HIV monoclonal antibodies and immune sera by defining the mechanism of neutralization. Human antibodies. 2005; 14:101–113. [PubMed: 16720980]
38. Cardoso RM, Zwick MB, Stanfield RL, Kunert R, Binley JM, Katinger H, Burton DR, Wilson IA. Broadly neutralizing anti-HIV antibody 4E10 recognizes a helical conformation of a highly conserved fusion-associated motif in gp41. Immunity. 2005; 22:163–173. published online EpubFeb. [PubMed: 15723805]
39. Frey G, Peng H, Rits-Volloch S, Morelli M, Cheng Y, Chen B. A fusion-intermediate state of HIV-1 gp41 targeted by broadly neutralizing antibodies. Proceedings of the National Academy of Sciences of the United States of America. 2008; 105:3739–3744. published online EpubMar 11. [PubMed: 18322015]
40. Leaman DP, Lee JH, Ward AB, Zwick MB. Immunogenic Display of Purified Chemically Cross-Linked HIV-1 Spikes. Journal of virology. 2015; 89:6725–6745. published online EpubJul. [PubMed: 25878116]
41. Chen J, Frey G, Peng H, Rits-Volloch S, Garrity J, Seaman MS, Chen B. Mechanism of HIV-1 neutralization by antibodies targeting a membrane-proximal region of gp41. Journal of virology. 2014; 88:1249–1258. published online EpubJan. [PubMed: 24227838]
42. Guenaga J, Dosenovic P, Ofek G, Baker D, Schief WR, Kwong PD, Karlsson Hedestam GB, Wyatt RT. Heterologous epitope-scaffold prime:boosting immuno-focuses B cell responses to the HIV-1 gp41 2F5 neutralization determinant. PloS one. 2011; 6:e16074. [PubMed: 21297864]
43. Ofek G, Guenaga FJ, Schief WR, Skinner J, Baker D, Wyatt R, Kwong PD. Elicitation of structure-specific antibodies by epitope scaffolds. Proceedings of the National Academy of Sciences of the United States of America. 2010; 107:17880–17887. published online EpubOct 19. [PubMed: 20876137]
44. Suloway C, Pulokas J, Fellmann D, Cheng A, Guerra F, Quispe J, Stagg S, Potter CS, Carragher B. Automated molecular microscopy: the new Leginon system. Journal of structural biology. 2005; 151:41–60. published online EpubJul. [PubMed: 15890530]
45. Li X, Mooney P, Zheng S, Booth CR, Braunfeld MB, Gubbens S, Agard DA, Cheng Y. Electron counting and beam-induced motion correction enable near-atomic-resolution single-particle cryo-EM. Nature methods. 2013; 10:584–590. published online EpubJun. [PubMed: 23644547]
46. Voss NR, Yoshioka CK, Radermacher M, Potter CS, Carragher B. DoG Picker and TiltPicker: software tools to facilitate particle selection in single particle electron microscopy. Journal of structural biology. 2009; 166:205–213. published online EpubMay. [PubMed: 19374019]
47. Mindell JA, Grigorieff N. Accurate determination of local defocus and specimen tilt in electron microscopy. Journal of structural biology. 2003; 142:334–347. published online EpubJun. [PubMed: 12781660]

48. Ogura T, Iwasaki K, Sato C. Topology representing network enables highly accurate classification of protein images taken by cryo electron-microscope without masking. Journal of structural biology. 2003; 143:185–200. published online EpubSep. [PubMed: 14572474]

49. Scheres SH. A Bayesian view on cryo-EM structure determination. Journal of molecular biology. 2012; 415:406–418. published online EpubJan 13. [PubMed: 22100448]

50. Scheres SH. RELION: implementation of a Bayesian approach to cryo-EM structure determination. Journal of structural biology. 2012; 180:519–530. published online EpubDec. [PubMed: 23000701]

51. Sorzano CO, Bilbao-Castro JR, Shkolnisky Y, Alcorlo M, Melero R, Caffarena-Fernandez G, Li M, Xu G, Marabini R, Carazo JM. A clustering approach to multireference alignment of single-particle projections in electron microscopy. Journal of structural biology. 2010; 171:197–206. published online EpubAug. [PubMed: 20362059]

52. Frank J, Penczek P, Liu W. Alignment, classification, and three-dimensional reconstruction of single particles embedded in ice. Scanning microscopy. Supplement. 1992; 6:11–20. discussion 20-12. [PubMed: 1366339]

53. Song Y, DiMaio F, Wang RY, Kim D, Miles C, Brunette T, Thompson J, Baker D. High-resolution comparative modeling with RosettaCM. Structure. 2013; 21:1735–1742. published online EpubOct 8. [PubMed: 24035711]

54. Emsley P, Cowtan K. Coot: model-building tools for molecular graphics. Acta crystallographica. Section D, Biological crystallography. 2004; 60:2126–2132. published online EpubDec. [PubMed: 15572765]

55. DiMaio F, Song Y, Li X, Brunner MJ, Xu C, Conticello V, Egelman E, Marlovits TC, Cheng Y, Baker D. Atomic-accuracy models from 4.5-A cryo-electron microscopy data with density-guided iterative local refinement. Nature methods. 2015; 12:361–365. published online EpubApr. [PubMed: 25707030]

56. DiMaio F, Tyka MD, Baker ML, Chiu W, Baker D. Refinement of protein structures into low-resolution density maps using rosetta. Journal of molecular biology. 2009; 392:181–190. published online EpubSep 11. [PubMed: 19596339]

57. Kucukelbir A, Sigworth FJ, Tagare HD. Quantifying the local resolution of cryo-EM density maps. Nature methods. 2014; 11:63–65. published online EpubJan. [PubMed: 24213166]

58. Woods RJ, Pathiaseril A, Wormald MR, Edge CJ, Dwek RA. The high degree of internal flexibility observed for an oligomannose oligosaccharide does not alter the overall topology of the molecule. European journal of biochemistry / FEBS. 1998; 258:372–386. published online EpubDec 1. [PubMed: 9874202]

59. Lutteke T, von der Lieth CW. pdb-care (PDB carbohydrate residue check): a program to support annotation of complex carbohydrate structures in PDB files. BMC bioinformatics. 2004; 5:69. published online EpubJun 4. [PubMed: 15180909]

60. Rillahan CD, Antonopoulos A, Lefort CT, Sonon R, Azadi P, Ley K, Dell A, Haslam SM, Paulson JC. Global metabolic inhibitors of sialyl- and fucosyltransferases remodel the glycome. Nature chemical biology. 2012; 8:661–668. published online EpubJul. [PubMed: 22683610]

61. Lander GC, Stagg SM, Voss NR, Cheng A, Fellmann D, Pulokas J, Yoshioka C, Irving C, Mulder A, Lau PW, Lyumkis D, Potter CS, Carragher B. Appion: an integrated, database-driven pipeline to facilitate EM image processing. Journal of structural biology. 2009; 166:95–102. published online EpubApr. [PubMed: 19263523]

62. Yang Z, Fang J, Chittuluru J, Asturias FJ, Penczek PA. Iterative stable alignment and clustering of 2D transmission electron microscope images. Structure. 2012; 20:237–247. published online EpubFeb 8. [PubMed: 22325773]

63. Tang G, Peng L, Baldwin PR, Mann DS, Jiang W, Rees I, Ludtke SJ. EMAN2: an extensible image processing suite for electron microscopy. Journal of structural biology. 2007; 157:38–46. published online EpubJan. [PubMed: 16859925]

64. Penczek PA, Grassucci RA, Frank J. The ribosome at improved resolution: new techniques for merging and orientation refinement in 3D cryo-electron microscopy of biological particles. Ultramicroscopy. 1994; 53:251–270. published online EpubMar. [PubMed: 8160308]

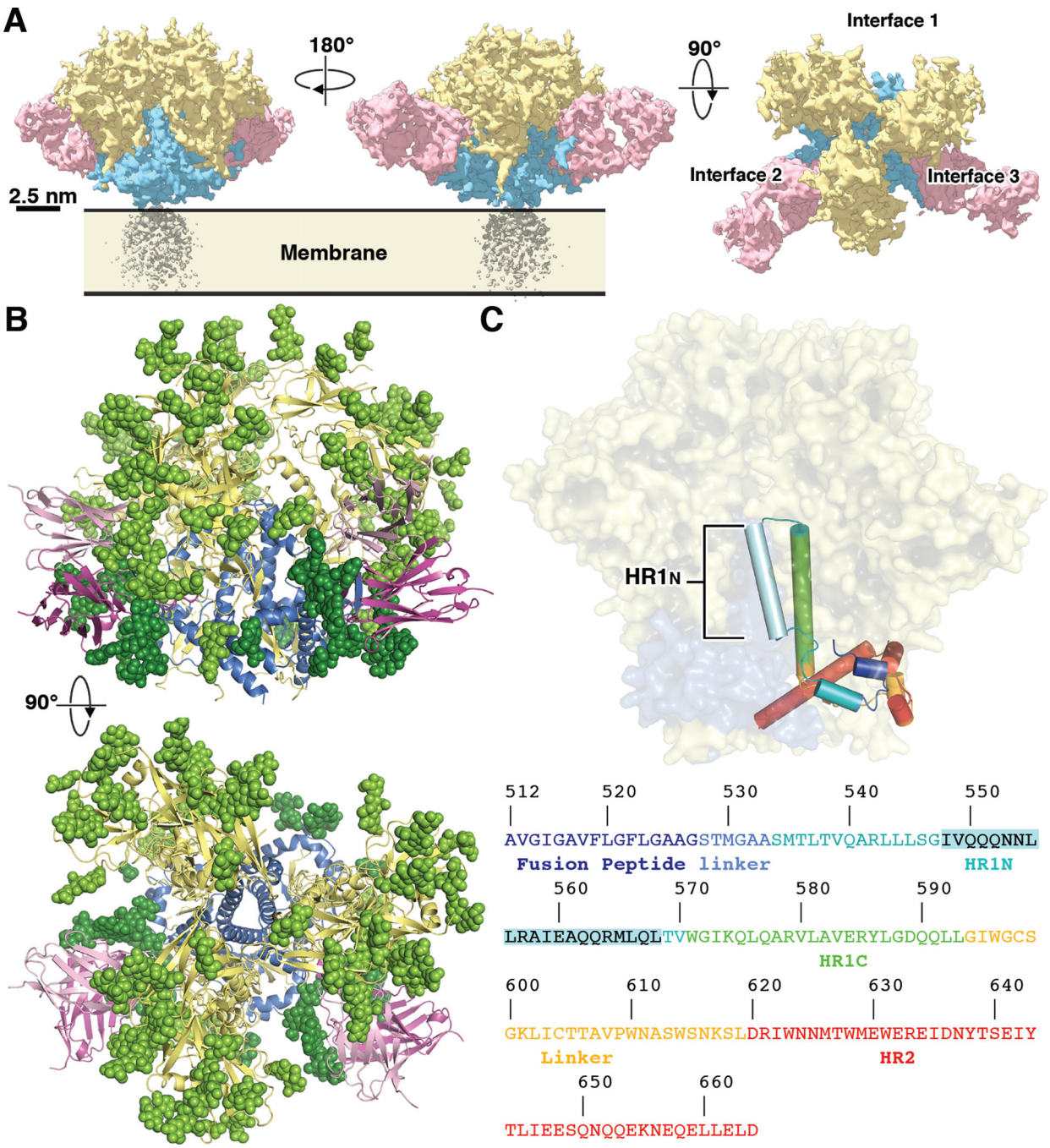

Fig. 1. CryoEM reconstruction of JR-FL EnvΔCT

(**A**) Reconstruction of JR-FL EnvΔCT in complex with PGT151 Fab at 4.2 Å resolution, segmented to highlight densities corresponding to gp120 (yellow), gp41 (blue), PGT151 Fab (pink), and the micelle surrounding the MPER and TM domain (gray). The three possible PGT151 binding sites are labeled as interface 1 (unliganded), interface 2, and interface 3. **(B)** Model of the EnvΔCT ectodomain, colored as in (A). The Fab LC and HC are colored in pink and magenta, respectively. Glycans are shown as spheres, with the gp120 and gp41 glycans shown in light and dark green, respectively. (**C**) Simplified cartoon rendering of

gp41. Most of HR1 (residues 534–593) that is missing in the x-ray structure (residues 548–568) is here revealed to be an α-helix. To distinguish this region from the central HR1 helix (residues 571–593), we call these two helices $HR1_N$ and $HR1_C$, respectively. The complete HR1 spans residues 534–593. The cartoon cylinder and loops are colored according to the sequence shown at the bottom.

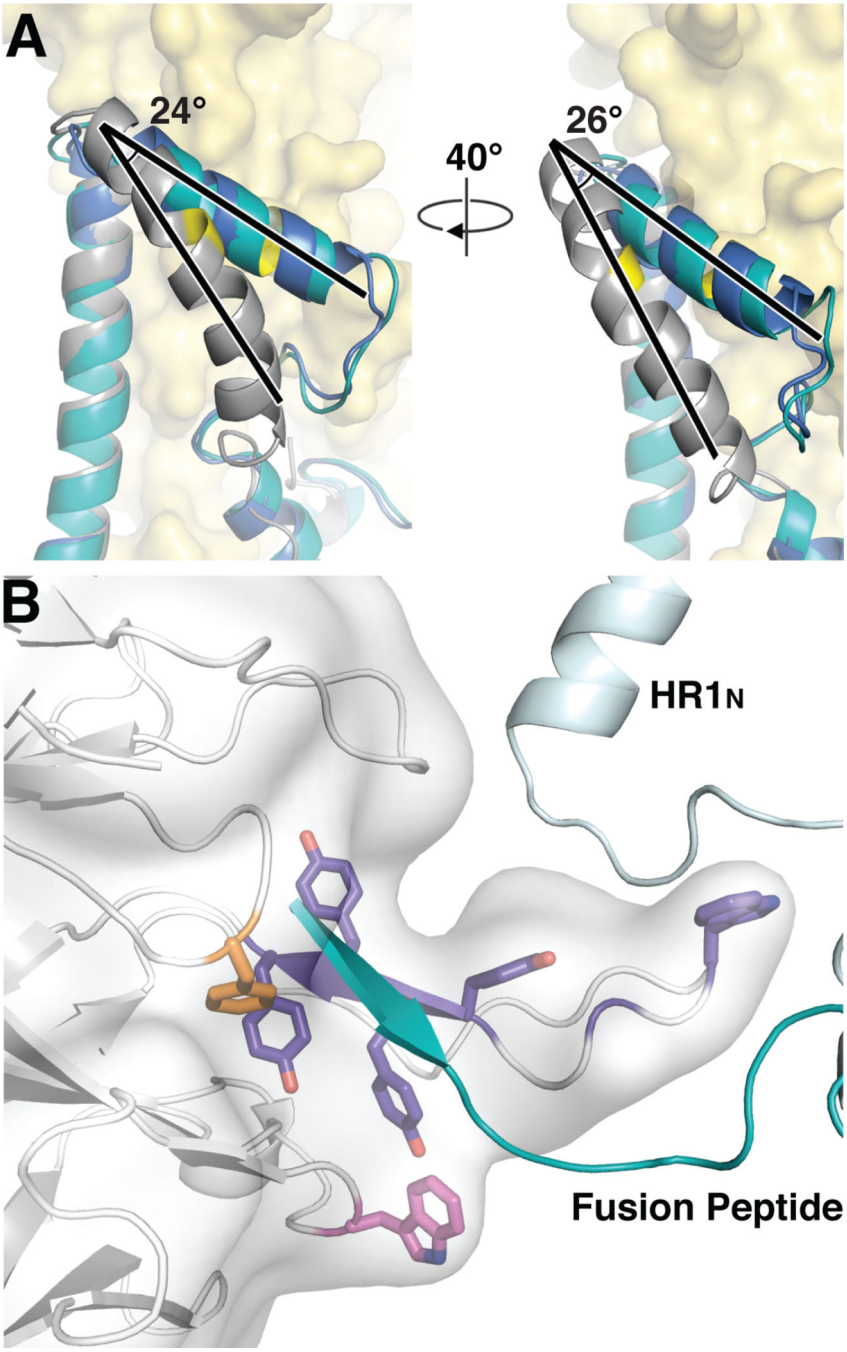

Figure 2. Conformational changes induced by PGT151 binding

(**A**) Compared to interface 1 (gray), $HR1_N$ in interface 2 (blue) and 3 (teal) are shifted about 24° outwards towards the Env surface, and 26° towards gp120 of the same protomer (yellow surface). The position of I559 residue is shown in yellow. (**B**) The FP (teal) is inserted into a hydrophobic pocket formed by the PGT151 CDR loops (CDRH2: magenta, CDRH3: purple, CDRL3: orange). The hydrophobic aromatic residues are shown as sticks.

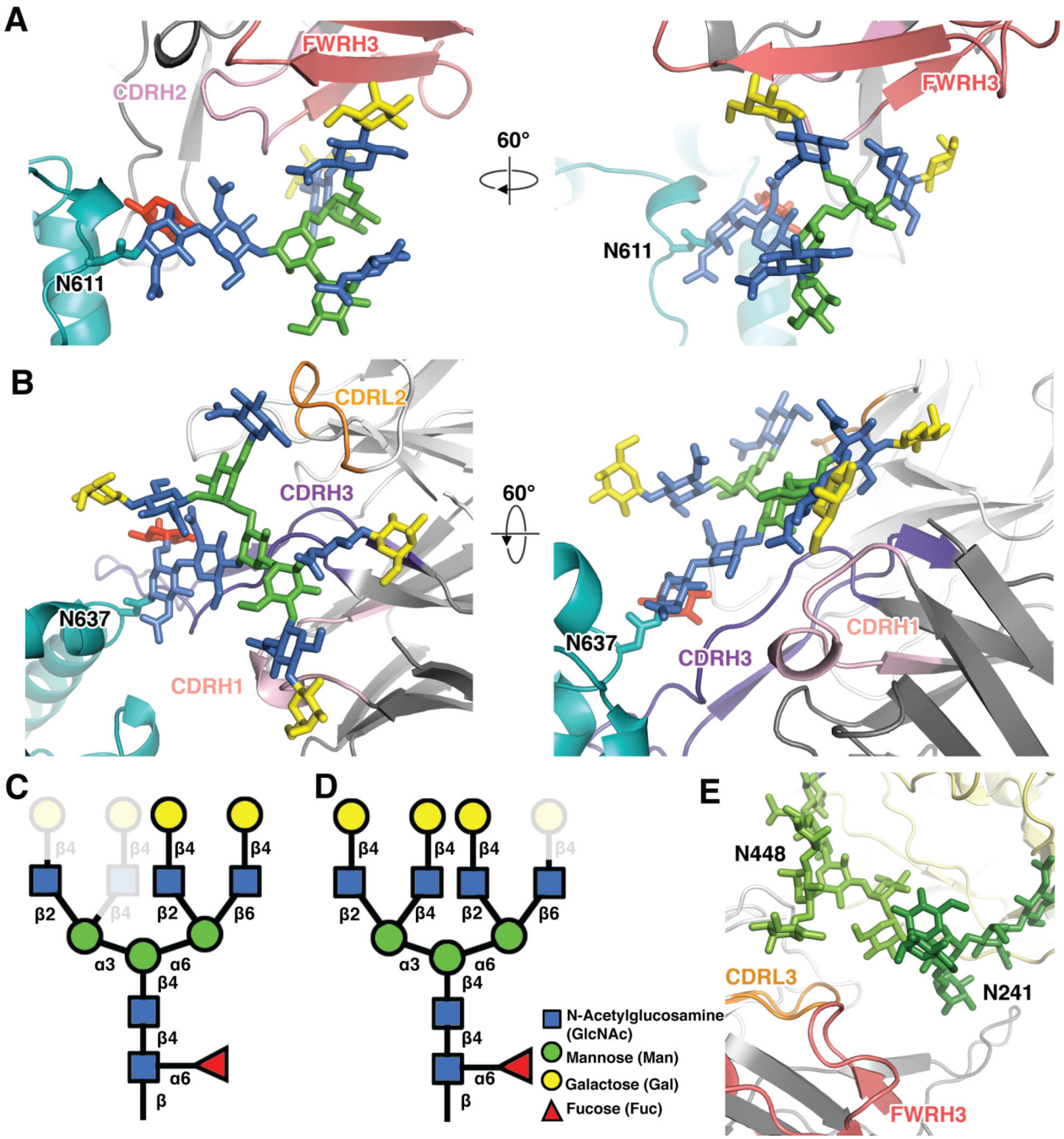

Figure 3. Glycan structures on the Env trimer

(A) The glycan at position N611 makes extensive contacts with PGT151 Fab. The glycan residues are colored according to the diagram in (C). **(B)** As in (A) but for the N637 glycan. The glycans modeled at N611 **(C)** and N637 **(D)** The dark shades represent sugar moieties resolved in the current structure while the light shades represent inferred sugars that are disordered. **(E)** The N241 and N448 glycans (different shades of green) are in close proximity to CDRL3 and FWRH3 of PGT151.

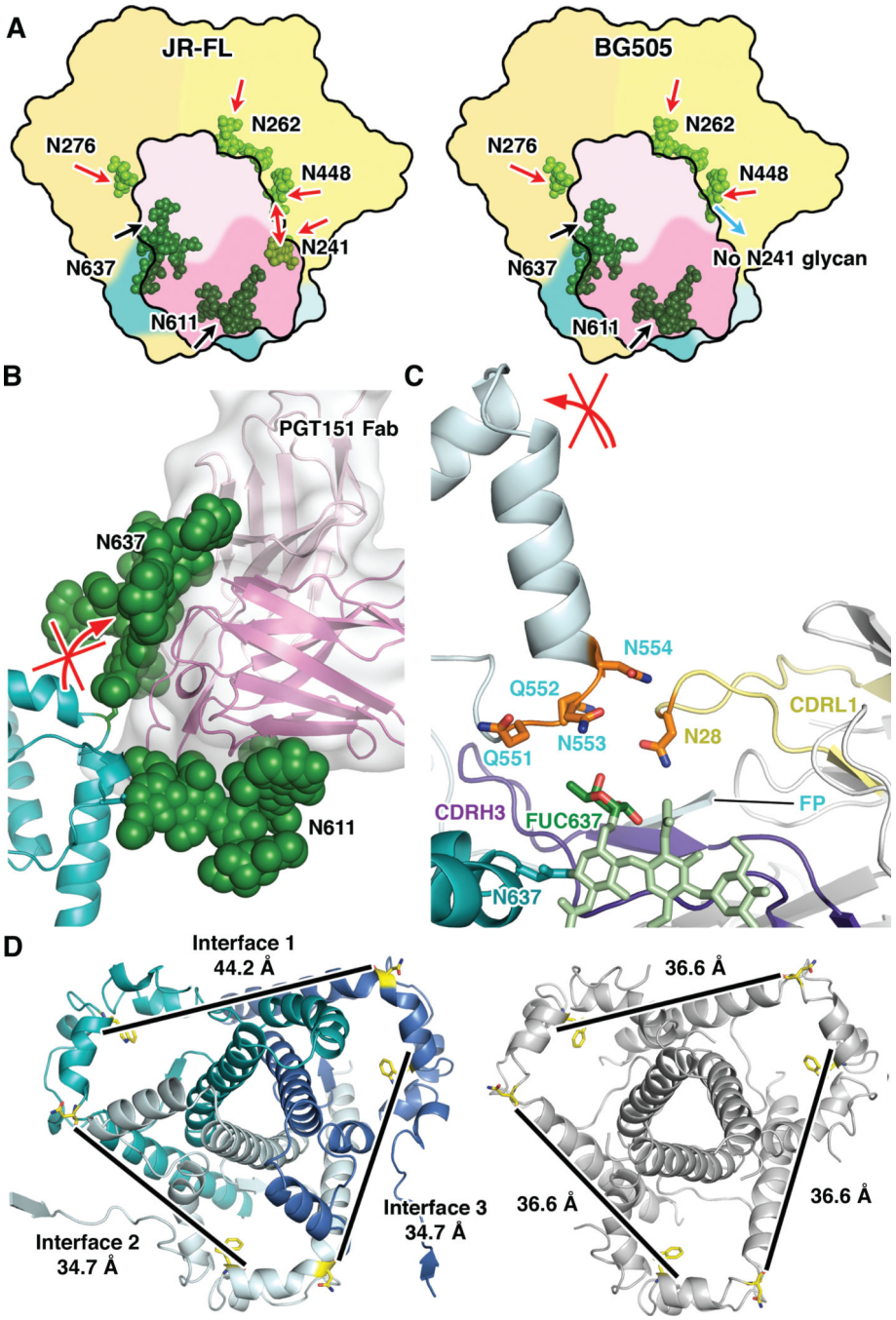

Figure 4. The complete PGT151 epitope

(**A**) A model of PGT151 and glycan interactions. Glycans from up to four different subunits (two gp120, two gp41) from two protomers of the trimer can lock the Fab in its bound form (left). Some of the glycans bind PGT151 with high affinity (black arrows), but there are numerous steric barriers that need to be overcome (red arrows). Glycans N241 and N448 likely have an inhibitory effect on PGT151 binding by influencing the conformations of each other. Lack of the N241 glycan (right) alleviates steric pressure by N448 (blue arrow). Different gp120 subunits are shown in shades of yellow, gp41 subunits in shades of blue,

Fab LC and HC in pink and magenta, gp120 glycans in green, and gp41 glycans in dark green. **(B)** When PGT151 is bound to glycans at N611 and N637, HR2 is locked in a bent conformation, and therefore cannot undergo conformational changes into the extended post-fusion form. (**C**) PGT151 CDRL1 (yellow) and the N637 glycan fucose (dark green) interact with a Glu/Asn rich region of $HR1_N$ on the adjacent gp41 (blue). The CDRH3 (purple) inserts between $HR1_N$ and the FP, and these interactions cap $HR1_N$ to lock gp41 in the prefusion conformation. The interacting residues in the Fab and $HR1_N$ are shown in orange. Only the core Man(Fuc)$GlcNAc_2$ residues are shown for the N637 glycan for clarity. (**D**) A measurement of the inter-gp41 distances in PGT151 bound JR-FL (left) compared to the unliganded BG505 trimer (right). Relative to the unliganded BG505 trimer which measures ~37 Å between Cα of N628 and N637 on the adjacent protomer, the distance between the same two residues measures ~35 Å at the PGT151 liganded interfaces. On the other hand, the inter-gp41 distance at interface 1 (~44 Å) is ~9 Å further apart in comparison to the liganded interfaces, indicating that the trimer becomes asymmetric in the PGT151-bound form.

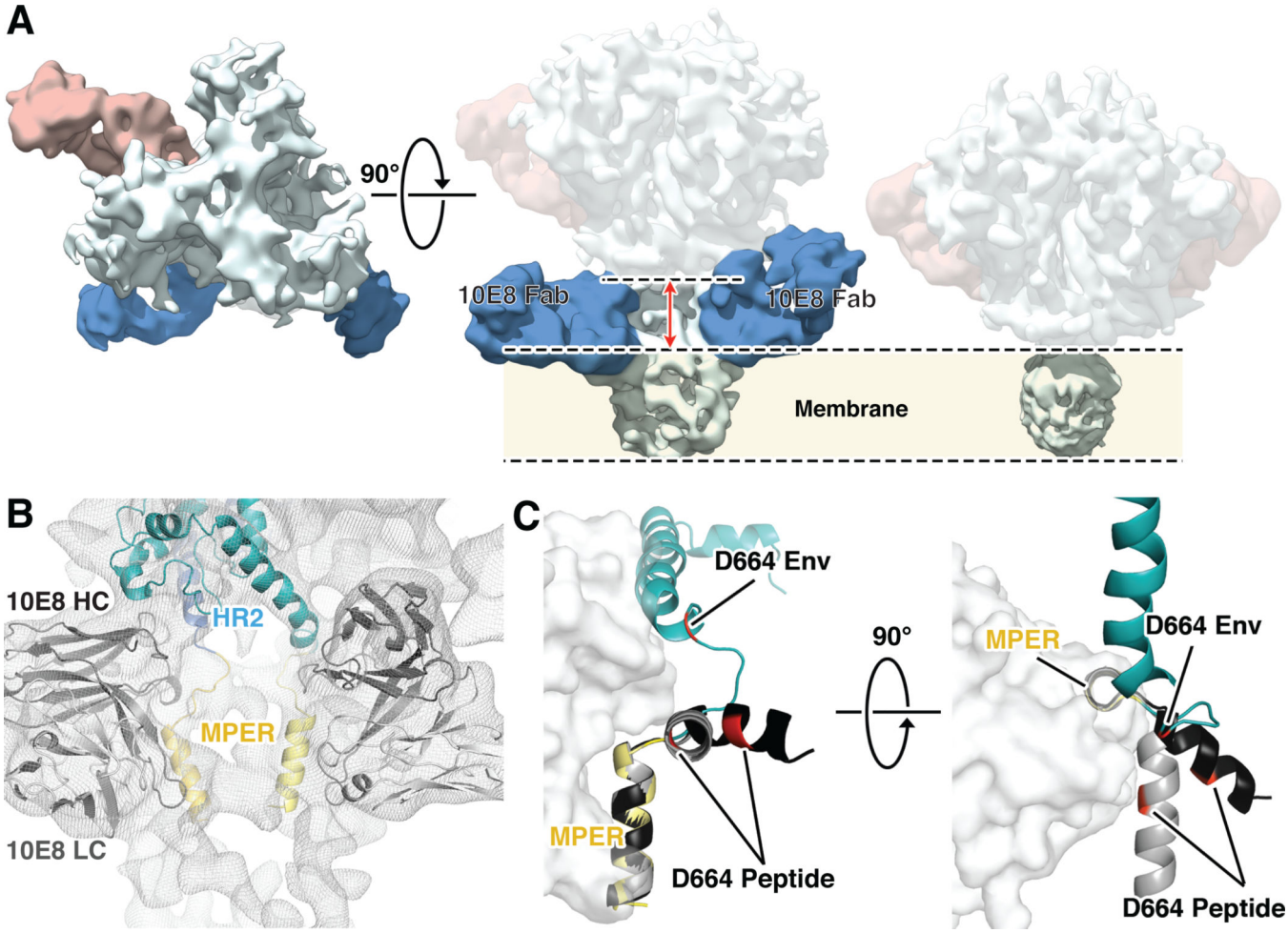

Figure 5. JR-FL EnvΔCT bound to PGT151 and 10E8

(**A**) CryoEM reconstruction of JR-FL EnvΔCT in complex with both PGT151 and the MPER binding antibody 10E8 at 8.8 Å resolution (left). The JR-FL EnvΔCT-PGT151 reconstruction low-pass filtered to 8.8 Å is shown on the right for comparison. The reconstructions indicate that when 10E8 is bound, the trimer is lifted off the membrane (red arrow), suggesting a conformational change in the MPER/TM. (**B**) The Env HR2-MPER connectivity in 10E8-bound form is modeled into the EM density. (**C**) A comparison of the position of residues 659–670 in the two asymmetric units (ASU) of the 10E8 bound MPER peptide x-ray model (dark and light gray), superimposed on the complete Env model (blue), in which the primary MPER epitope (residues 671–685) is shown in yellow. This N-terminal segment exhibits different conformations in the two ASUs. D664 is colored in red as a point of reference. 10E8 is shown as the white surface.

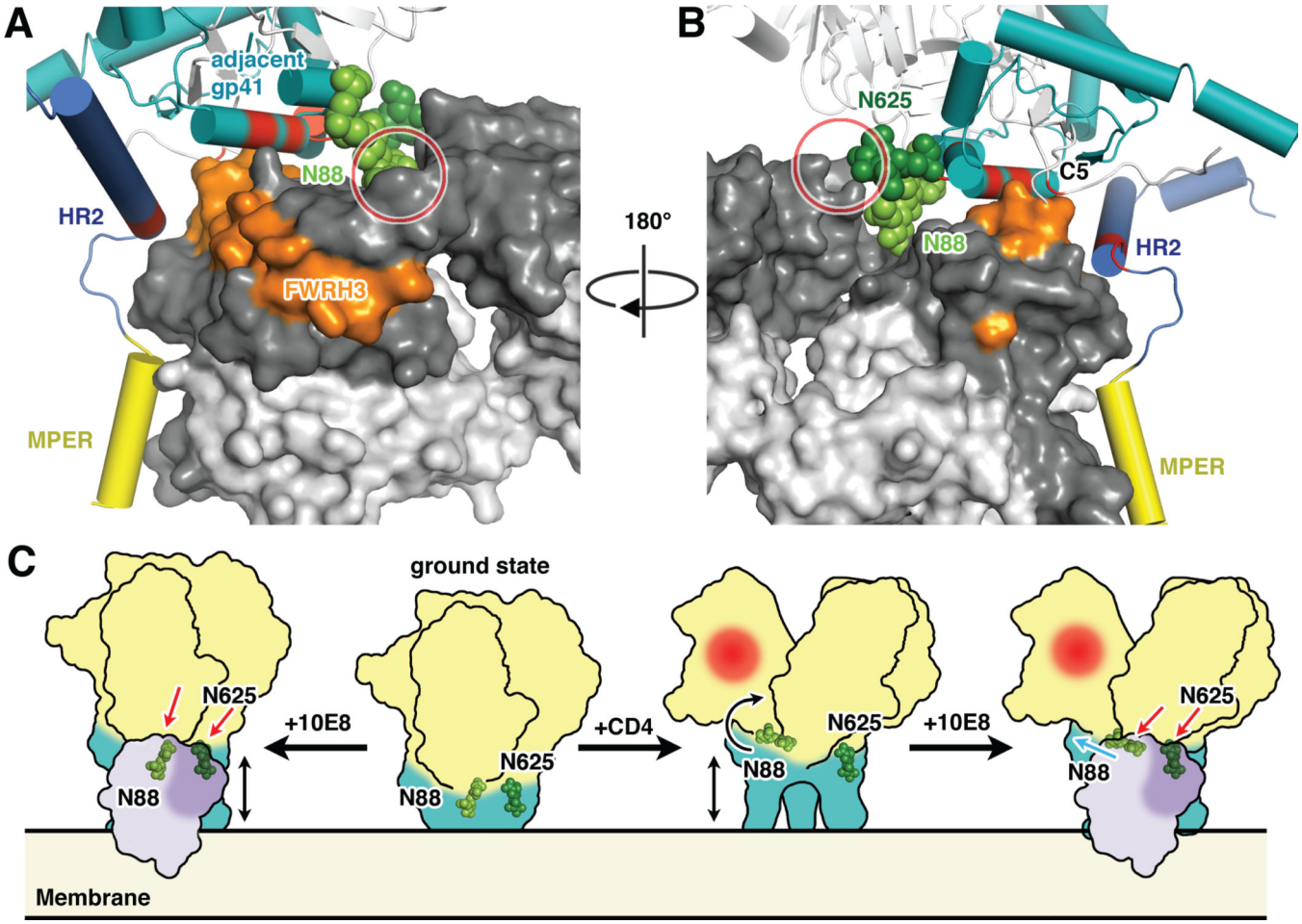

Figure 6. 10E8 contact analysis in the context of the Env ectodomain

(**A**) and (**B**) A model of the 10E8 epitope in the context of the intact Env trimer. The Fab constant region and the nearby Env gp120 is also shown. In blue is the gp41 that the 10E8 Fab makes primary interactions with the MPER residues 671–685 (yellow). Additional contacts could be made with the HR2 and C-terminal region of the FP in the adjacent gp41 (teal), as well as regions in gp120 (white). These additional contacts to Env within a 4 Å radius of 10E8 are shown in red. Many of these interactions are likely FRWH3 (orange) mediated. The model also demonstrates that the N88 (A), and N625 (B) glycans could sterically obstruct 10E8 binding. The glycans modeled here are $ManGlcNAc_2$ for N88 and GlcNAc for N625 (Table S1), but are expected to be larger in native Env. (**C**) Glycans at N88 and N625 sterically hinder 10E8 binding to the trimer (left, red arrows). Binding of 10E8 (left) or CD4 (center right) lifts the MPER up from the membrane, relative to the ground state (center left). In the CD4-bound conformation, the opening of the trimers results in rotation of the gp120s, moving N88 away from the 10E8 binding site relieving some steric hindrance (right, blue arrow).